ORGANOMETALLICS

Article

pubs.acs.org/Organometallics

Subvalent Iridium Precursors for Atom-Efficient Chemical Vapor Deposition of Ir and IrO_2 Thin Films

Lasse Jürgensen, Michael Frank, Myeongwhun Pyeon, Lisa Czympiel, and Sanjay Mathur*

Institute of Inorganic Chemistry, University of Cologne Greinstrasse 6, D-50939 Cologne, Germany

Supporting Information

ABSTRACT: A new heteroleptic Ir(I) compound exhibiting high volatility and defined thermal decomposition under CVD conditions is reported. The new iridium precursor [(COD)Ir(ThTFP)] (COD = cyclooctadiene, ThTFP = (*Z*)-3,3,3-trifluoro-1-(thiazol-2-yl)prop-1-en-2-olate) unifies both reactivity and sufficient stability through its heteroleptic constitution to provide a precise control over compositional purity in CVD deposits. The solution integrity of the monomeric Ir(I) complex was investigated by 1D and 2D NMR spectroscopy and EI mass spectrometry, whereas the molecular structure was confirmed by single-crystal diffraction. CVD experiments demonstrated the suitability of the iridium compound for an atom-efficient (high molecule-to-precursor yield) gas-phase deposition of nanocrystalline iridium films that could be converted into crystalline iridium dioxide upon heat treatment to demonstrate their electrocatalytic potential in the oxygen evolution reaction.

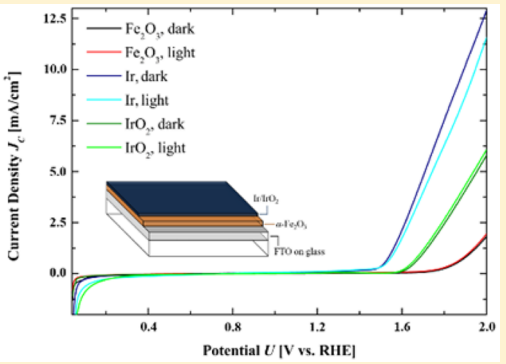

INTRODUCTION

Iridium is one of the less earth-abundant elements; however, its physical and chemical properties are of growing interest,[1−3] especially due to the applications of iridium and iridium dioxide thin films in catalytic oxygen evolution reactions (OER) and optoelectronic applications.[4−15] The superior hardness and interesting conducting properties of iridium and iridium dioxide demand new methods to produce iridium-based thin films in an economical and ecological way.[16−18] In this context, the chemical vapor deposition (CVD) process offers a promising solution, which however requires molecular compounds with substantial vapor pressure essential to achieve iridium feedstock in the gas phase.[19−21] Typically, known metal−organic compounds such as metal alkoxide, metal carbonyl, or β-diketonate complexes are used that suffer from low vapor pressure and decomposition temperatures, thereby providing little control over film growth conditions.[17,22−25] Moreover, in many cases, the use of reactive gases is necessary to accelerate the precursor in the gas phase.[17,25] The necessary volatility of precursors strongly depends on inter- and intramolecular interactions as well as the molecular weight of the compound. To decrease molecular weight and increase volatility, small ligands such as methyl groups are desired for the synthesis of precursors. Because of their low steric demand, these precursors are kinetically labile. Application of neutral chelating ligands should increase the stability of the complexes and allow a careful design of heteroleptic precursors showing sufficient volatility and adequate reactivity (Scheme 1).[26−30]

We report herein the solid-state and solution-phase structure of the new heteroleptic iridium(I) precursor [(COD)Ir(ThTFP)] (**3**) and demonstrate its intrinsic advantages as a molecular precursor for the phase-selective synthesis of iridium-based films via CVD. Furthermore, quantitative conversion of nanocrystalline iridium films into phase-pure iridium dioxide films and their electrocatalytic behavior is described.

Scheme 1. Janus-Headed Precursors To Combine Structural Stability with Electronic Flexibility

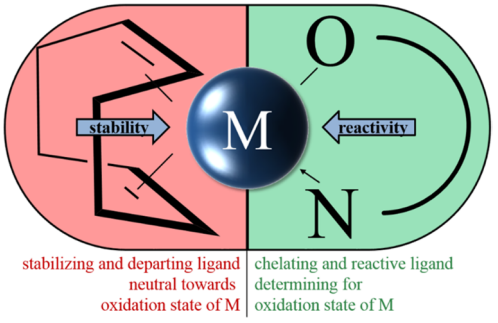

RESULTS AND DISCUSSION

Precursor Synthesis. The bidentate ligand HThTFP (**1**) was prepared by reacting 2-methylthiazole with trifluoroacetic acid anhydride in the presence of pyridine under elimination of pyridinium trifluoroacetate. The heteroleptic iridium(I) precursor [(COD)Ir(ThTFP)] (**3**) was synthesized via a salt metathesis reaction (Scheme 2) by reacting dimeric $[(COD)IrCl]_2$ (**2**) and the sodium salt of **1** (NaThTFP, **1b**).[31]

Received: April 14, 2017

DOI: 10.1021/acs.organomet.7b00275
Organometallics XXXX, XXX, XXX−XXX

Scheme 2. Synthetic Route to Bidentate Ligand HThTFP (1) and Heteroleptic Iridium(I) Precursor [(COD)Ir(ThTFP)] (3)

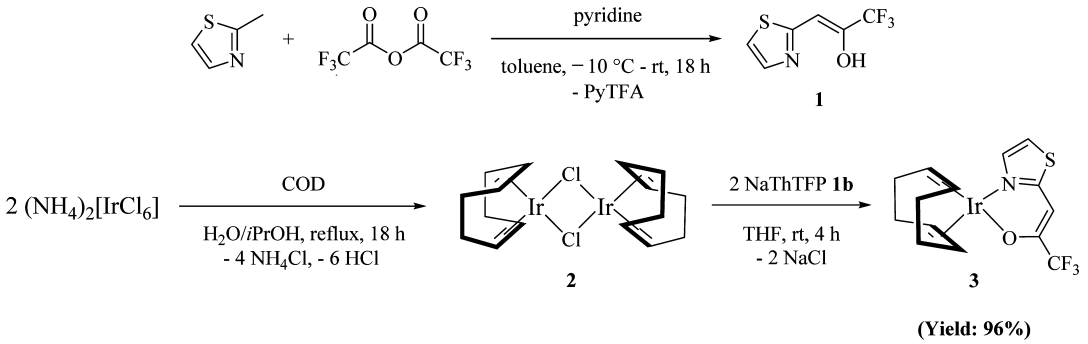

The heteroleptic iridium(I) complex **3** was isolated as an air-stable red-orange solid by sublimation under dynamic vacuum (110 °C, 10^{-3} mbar). The sublimation temperature of **3** is significantly lower than that for Ir(acac)$_3$ (180 °C, 10^{-3} mbar),[25] which is conventionally used as a precursor in the CVD of Ir(0) films. The higher volatility of [(COD)Ir-(ThTFP)] is attributed to the lower molecular weight and a lesser ionic character, as verified by the bond lengths determined through crystal structure analysis (see below).

Structural Characterization of [(COD)Ir(ThTFP)] (3). ^{1}H NMR and ^{1}H,^{1}H NOESY spectra (Figure 1; for additional NMR spectra see the Supporting Information) display two doublets at δ 7.21 ppm (^3J = 3.9 Hz) and δ 6.97 ppm (^3J = 3.9 Hz) corresponding to aromatic protons 1-H and 2-H. The vinylic proton 4-H in **3** appeared at δ 6.28 ppm as a sharp singlet. The unsaturated protons of COD (7-H) were observed as multiplets at δ 4.35 and 3.70 ppm, whereas the saturated part of COD exhibits multiplets shifted more upfield at δ 2.31 and 1.76 ppm. The ^{1}H,^{1}H NOESY spectrum (Figure 1) exhibits through-space coupling of 1-H and unsaturated protons of COD (7-H) (Figure 1, red circles), where the intensities of each signal indicate the exact ligand arrangement around the central iridium atom.

Single-crystal X-ray diffraction analysis of the heteroleptic iridium(I) complex **3** showed a distorted-square-planar coordination around iridium, as observed in other iridium(I) compounds.[32,33] The distorted geometry originated from the angle between the COD ligand and nitrogen atom N1, COD−Ir01−N1 96.153 ± 0.417°, which is much larger than the COD−Ir01−O1 angle of 86.883 ± 0.344° due to the higher steric profile of COD and hydrogen bonding between the enolic oxygen of ThTFP and hydrogen of the COD ligand (distance 2.627 ± 0.021 Å). This effect is augmented by the steric repulsion between the unsaturated parts of both ThTFP and COD ligands.

Compound **3** was investigated by EI mass spectrometry at an ionization energy of 70 eV and an evaporation temperature of 100 °C (10^{-6} mbar). The mass spectrum was dominated by the molecular ion $[M]^{\bullet+}$ at m/z 495 with an intensity of 100%. The thermal behavior of the precursor investigated by thermogravimetric (TG) analysis (Figure 2, left) showed a distinctive two-stage decomposition starting at 200 °C. The TG curve showed a first mass loss of 45 wt % which corresponded well to the loss of ThTFP. Further heating of the sample resulted in the removal of COD, passing a plateau (Figure 2, 600−700 °C) due to the increased stability of the COD-Ir species in the gas phase, yielding pure iridium metal at 40 wt % (theoretical 39 wt %) at 1000 °C. The Janus-type precursor concept described in Scheme 1 was confirmed by a distinctive two-stage thermal

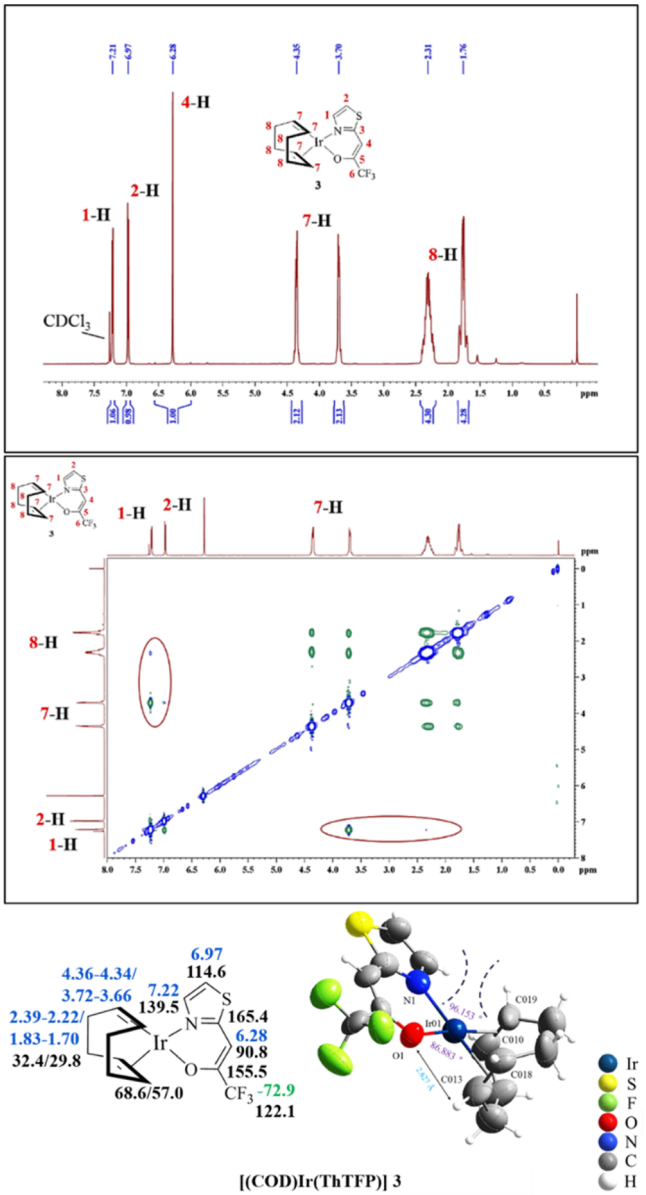

[(COD)Ir(ThTFP)] 3

Figure 1. (top) ^{1}H NMR and ^{1}H,^{1}H NOESY spectra (δ in ppm) of heteroleptic Ir(I) compound **3** (^{1}H (blue), ^{13}C (black), ^{19}F (green)), measured in $CDCl_3$. (bottom) Molecular structure of [(COD)Ir-(ThTFP)] (**3**). Thermal ellipsoids are drawn at the 50% probability level.

decomposition. The powder XRD data of the obtained metallic residue (Figure 2, right) revealed characteristic diffraction peaks

DOI: 10.1021/acs.organomet.7b00275
Organometallics XXXX, XXX, XXX−XXX

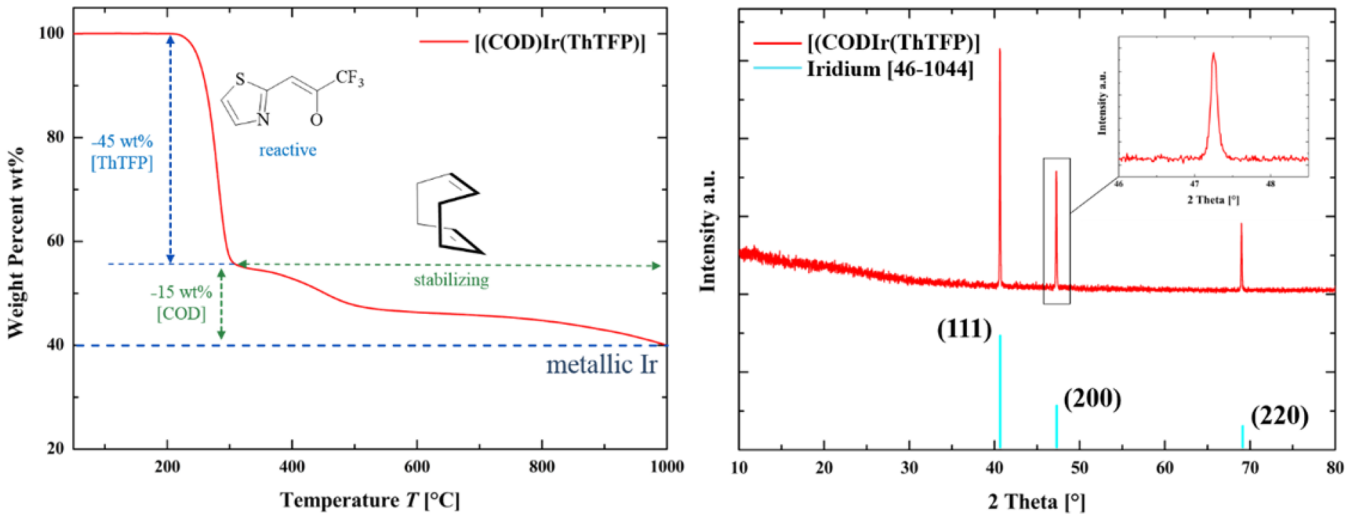

Figure 2. Thermogravimetric curve of heteroleptic Ir(I) compound **3** (left, red line) and obtained XRD pattern of the metallic residue (right).

(ICSD: 46-1044) for metallic iridium and confirmed the residue to be nanocrystalline iridium with an average size of 93 ± 4 nm (Scherer equation).

Chemical Vapor Deposition of [(COD)Ir(ThTFP)]. Phase-pure elemental iridium thin films were deposited on silicon and aluminum oxide substrates by decomposition of [(COD)Ir-(ThTFP)] (**3**) in a cold-wall reactor operating in the temperature range 700−800 °C with the precursor reservoir maintained at 110, 120, and 130 °C, whereas there is no sufficient precursor flow at 110 °C precursor temperature. XRD analysis showed that pure iridium phase (ICSD: 46-1044) was obtained at 800 °C for deposition times of 60 min (Figure 3), whereas the CVD deposits were mostly amorphous at lower substrate temperatures (Figure 3). The scanning electron micrographs unambiguously showed a homogeneous coating of amorphous iridium. Increasing the deposition time from 60 to 120 and 240 min enhanced the crystallinity even at 700 °C to provide nanocrystalline iridium(0) coatings. Therefore, the deposition time has more influence on the crystallinity of the coatings than the precursor temperature. Additionally, no disproportionation reactions of subvalent Ir(I) precursor to elemental iridium and iridium(IV) or iridium(III) oxides were noticed in XRD patterns, that indicated a defined deposition process.

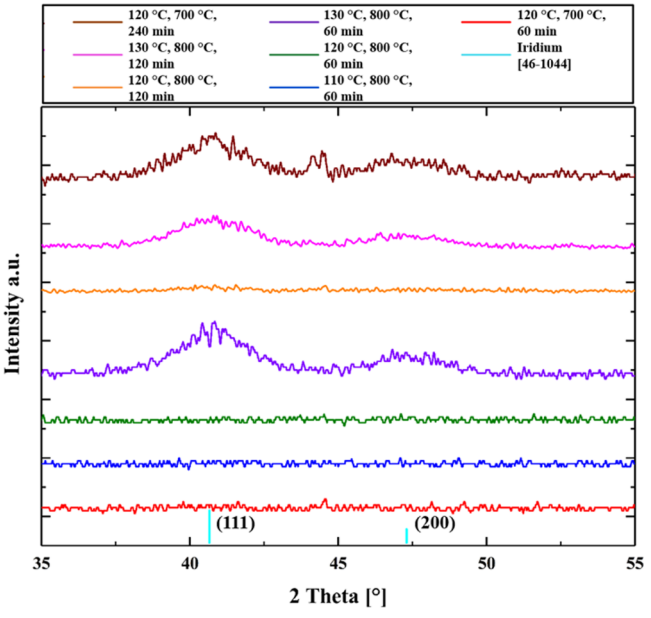

Figure 3. XRD patterns of iridium films deposited on Si substrates at different deposition parameters.

The successful deposition of iridium(0) films on single-crystal (Si), amorphous (SiO_2), and polycrystalline (Al_2O_3) substrates showed the universal applicability of the precursor and its chemically controlled decomposition irrespective of the surface chemistry of the substrate material (Figure 4; see XRD in the Supporting Information). The obtained micrographs depict homogeneous coatings of iridium nanoparticles all over the substrates (Figure 4, top left) with average diameters smaller than 30 nm. While the morphology of polycrystalline Al_2O_3 substrate is more inhomogeneous, nevertheless it was possible to observe a homogeneous coating all over the polycrystalline substrate. Cross-section images of the deposited films (see the Supporting Information) confirm a homogeneous coating throughout the whole substrate. With a precursor temperature of 120 °C and a substrate temperature of 700 °C a film thickness of 30 nm was achieved after a deposition time of 60 min. Further investigations concerning growth rate and influence of carrier or reactive gases on the deposition of iridium films are currently underway.

The annealing of iridium(0)-containing films on Si substrates for 5 h at 700 °C under ambient conditions induced the formation of phase-pure iridium dioxide films that were confirmed by X-ray diffractometry (ICSD: 15-0870, see the Supporting Information).

Application of Iridium-Containing Thin Films in Oxygen Evolution Application. The electrochemical activity of iridium layers was evaluated by a three-electrode system as depicted in Figure 5. To determine the potential of the synthesized Ir/IrO_2 films in photoelectrochemical water splitting, they were deposited onto crystalline hematite (α-Fe_2O_3) and titanium oxide (TiO_2; see the Supporting Information) films deposited by a plasma-enhanced vapor deposition (PE-CVD) and their electrochemical performances were compared. Figure 5 (right) exhibits $J-V$ curves of the prepared photoelectrodes. The current densities of both Ir and IrO_2 overlayered photoelectrodes under illumination are almost the same as that in darkness, although a slight increase in

DOI: 10.1021/acs.organomet.7b00275
Organometallics XXXX, XXX, XXX−XXX

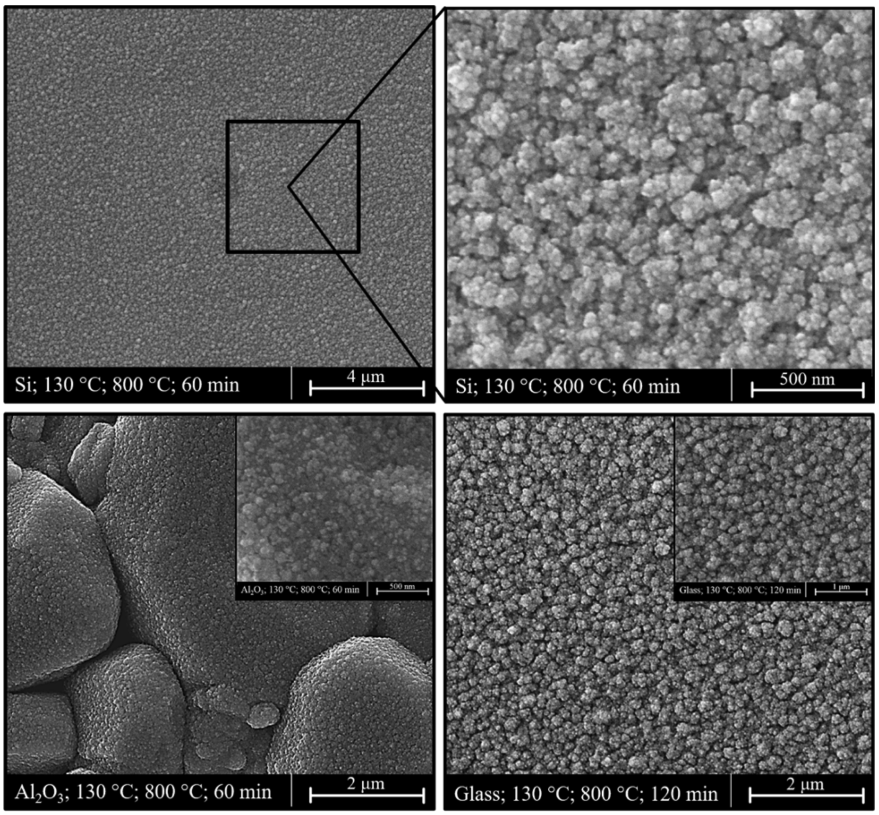

Figure 4. SEM images of iridium(0) films on Si (top), Al_2O_3 (bottom, left) and glass (bottom, right), deposited at different CVD parameters.

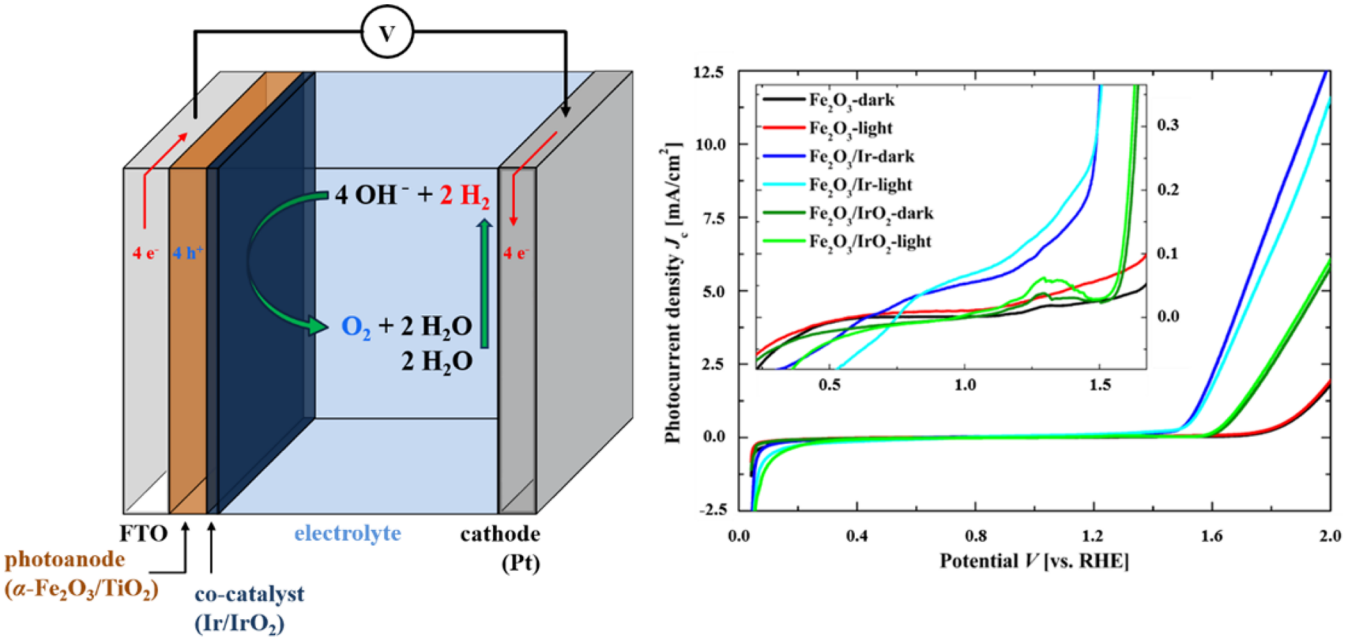

Figure 5. Schematic overview of a PEC cell (left) and dark and photocurrent densities J_C obtained from the prepared α-Fe_2O_3-containing photoelectrodes as a function of applied potential V (vs RHE) (right).

current density is observed under illumination (see the inset of Figure 5 (right)), which indicates that the overlayers of Ir and IrO_2 barely improve the photoactivity of hematite photoelectrodes. However, the onset potential, at which the current density starts rising, under dark conditions shifts in the cathodic (negative) direction gradually when the IrO_2 (~1.22 V vs RHE) and Ir (~0.75 V vs RHE) layers were deposited in comparison to the hematite photoelectrode (~1.40 V vs RHE). The onset potential values were determined by reading the potential at 0.02 mA/cm^2, although there are several methods to determine the onset potential.[34,35] This cathodic onset potential shift of dark current can be attributed to improved electrocatalytic activity.[36] Ir and IrO_2 films synthesized by a CVD process were stable under the measurement conditions

DOI: 10.1021/acs.organomet.7b00275
Organometallics XXXX, XXX, XXX−XXX

and seem to be promising for use as (photo)electrochemical catalysts. Further experiments involving TiO_2 as a photocatalytic layer and electrodes without photocatalyst (Ir/IrO_2 on FTO) have been performed and are currently underway (see the Supporting Information).[37]

CONCLUSION

Heteroleptic iridium(I) complexes containing both anionic and neutral multidentate ligands demonstrated a synergistic interplay of reactivity and stability (Scheme 1) essential for development of new precursors for gas-phase methods. This combination of less polar Ir−C bonds and coordinative Ir//N^O units enabled an atom-efficient and distinctive two-step decomposition mechanism. The coordination of bidentate β-heteroaryl-alkenolate and COD ligands on the iridium center produced an Ir(I) precursor with high volatility originating from a careful ligand design. The deposition of Ir(0) films on various substrate materials without the need for additional reactant gases underlines the potential of this precursor class for CVD and ALD of metallic thin films. The presented synthetic and CVD data open new possibilities in the vapor-phase synthesis of iridium-based materials facilitating the application of such films, for example, as electro- or photocatalysts in the OER.

EXPERIMENTAL SECTION

Chemicals and Methods. All manipulations of air- and moisture-sensitive materials were carried out under nitrogen using all glass assemblies. NMR spectra were recorded on a Bruker Avance II spectrometer operating at ^{1}H 300.1 MHz, ^{13}C 75.5 MHz, and ^{19}F 282.4 MHz; chemical shifts are given in parts per million (ppm) relative to TMS (^{1}H, ^{13}C) and $CFCl_3$ (^{19}F), and coupling constants (J) are given in Hz. NMR spectra have been plotted by Bruker TopSpin 3.2[38] software. Mass spectra were recorded on a Finnigan MAT 95 instrument (EI, 70 eV) in m/z (intensity in %). Data collection for X-ray structure elucidation was performed on a STOE IPDS II diffractometer using monochromated Mo Kα radiation (λ = 0.71071 Å). The programs used in this work are STOE's X-Area[39] and the WINGX suite of programs,[40] including SIR-92,[41] SHELX, and SHELXTL[42] and PLATON[43] for structure solution and refinement. H atoms were calculated geometrically, and a riding model was applied during the refinement process. TG measurements were performed on a TGA/DSC1 (METTLER-TOLEDO GmbH, Germany) apparatus.

Precursor Synthesis. *(Z)-3,3,3-Trifluoro-1-(thiazol-2-yl)prop-1-en-2-ol (**1**; HThTFP).* **1** was prepared by modifying the procedure described by Kawase et al.[44] A 2.97 g portion (30 mmol, 1.0 equiv) of 2-methylthiazole and 12.1 mL (150 mmol, 5.0 equiv) of pyridine were dissolved in 80 mL of toluene and cooled to 0 °C, and then 12.7 mL of trifluoroacetic acid anhydride (90 mmol, 3.0 equiv) was added dropwise. The mixture was stirred for 18 h at room temperature. Afterward 300 mL of 3% Na_2CO_3(aq) was added slowly and the mixture was extracted with EtOAc (4 × 200 mL). The combined organic phases were washed with brine solution (300 mL) and dried over $MgSO_4$, and the solvent was removed under reduced pressure. The crude product was purified by sublimation under dynamic vacuum (55 °C, 10^{-3} mbar) to obtain a yellowish solid (**1**). Yield: 63% (3.71 g). ^{1}H NMR (300.1 MHz, 298 K, DMSO-d_6): δ 13.20 (s, 1H, OH); 7.62 (d, $^3J_{H,H}$ = 4.0 Hz, 1H, 1-H); 7.13 (d, $^3J_{H,H}$ = 4.0 Hz, 1H, 2-H); 6.22 (s, 1H, 4-H). ^{19}F NMR (282.4 MHz, 298 K, $CDCl_3$): δ −74.3 ($^1J_{F,C}$ = 291 Hz, $^2J_{F,C}$ = 38 Hz). EI-MS (70 eV, 36 °C): m/z (intensity) 195 (68%) $[M]^+$, 126 (100%) $[M - CF_3]^+$, 98 (28%) $[C_4H_4NS]^+$, 58 (20%) $[C_2H_3S]^+$. Anal. Calcd for $C_6H_4F_3NOS$: C, 39.93; H, 2.07; N, 7.18; S, 16.43. Found: C, 37.12; H, 1.98; N, 8.01; S, 15.74.

*Sodium (Z)-3,3,3-Trifluoro-1-(thiazol-2-yl)prop-1-en-2-olate (**1b**; NaThTFP).* **1b** was prepared by reacting with NaOEt. Therefore, 0.023 g (1.0 mmol, 1.0 equiv) of sodium was added to 10 mL of ethanol. After the mixture was stirred for 30 min, 0.195 g (1.0 mmol, 1.0 equiv) of ThTFP (**1**) was added to the solution. After removal of the excess solvent, an off-white solid (**1b**) was obtained. Yield: 0.216 g (1.0 mmol, >99%). ^{1}H NMR (300.1 MHz, 298 K, DMSO-d_6): δ 7.38 (d, $^3J_{H,H}$ = 3.3 Hz, 1H, 1-H); 6.86 (d, $^3J_{H,H}$ = 3.3 Hz, 1H, 2-H); 5.82 (s, 1H, 4-H). ^{19}F NMR (282.4 MHz, 298 K, $CDCl_3$): δ −72.4 ($^1J_{F,C}$ = 293 Hz, $^2J_{F,C}$ = 36 Hz).

*[(COD)IrCl]$_2$ (**2**).* **2** was prepared following a modified procedure described by Tani et al.[31] To a stirred solution of 0.441 g of $(NH_4)_2[IrCl_6]$ (1.0 mmol, 1.0 equiv) in a 2:1 mixture of H_2O and isopropyl alcohol (15 mL) was slowly added 0.98 mL of cycloocta-1,5-diene (COD) (8.0 mmol, 8.0 equiv). The resulting solution was heated to reflux for 12 h, upon which a red-orange solid precipitated out. After it was cooled to room temperature, the reaction mixture was evaporated to dryness and the crude product was extracted with 20 mL of *n*-pentane. After decanting and removal of the excess solvent, a red-orange solid (**2**) was obtained. Yield: 0.470 g (0.70 mmol, 70%). ^{1}H NMR (300.1 MHz, 298 K, $CDCl_3$): δ 4.24−4.23 (m, 4H, 1-H); 2.29−2.24 (m, 4H, 2-H); 1.57−1.49 (m, 4H, 2-H). ^{13}C APT (75.5 MHz, 298 K, $CDCl_3$): δ 62.4 (C1); 31.9 (C2). Anal. Calcd for $C_{16}H_{24}Cl_2Ir_2$: C, 28.61; H, 3.60. Found: C, 29.12; H, 2.98.

*[(COD)Ir(ThTFP)] (**3**).* **3** was prepared by placing 1.5 mmol (2.1 equiv) of the sodium salt of compound **1** (**1b**) in a flask. Afterward 0.470 g (0.7 mmol, 1.0 equiv) of [(COD)IrCl]$_2$ (**2**) dissolved in 30 mL of anhydrous THF was added to the sodium compound (**1b**). The mixture was stirred for 4 h at room temperature. After removal of the solvent under reduced pressure, the crude product was sublimed under dynamic vacuum (110 °C, 10^{-3} mbar) to afford a yellow-orange solid (**3**). Yield: 0.662 g (1.34 mmol, 96%), ^{1}H NMR (300.1 MHz, 298 K, $CDCl_3$): δ 7.22 (d, $^3J_{H,H}$ = 3.9 Hz, 1H, 1-H); 6.97 (d, $^3J_{H,H}$ = 3.9 Hz, 1H, 2-H); 6.28 (s, 1H, 4-H); 4.36−4.34 (m, 2H, 7-H); 3.72−3.66 (m, 2H, 7-H); 2.39−2.22 (m, 4H, 8-H); 1.83−1.70 (m, 4H, 8-H). ^{13}C APT (75.5 MHz, 298 K, $CDCl_3$): δ 165.4 (C3); 155.5 (C5); 139.5 (C1); 122.1 (C6); 114.6 (C2); 90.8 (C4); 68.6 (C7); 57.0 (C7); 32.4 (C8); 29.8 (C8). ^{19}F NMR (282.4 MHz, 298 K, $CDCl_3$): δ −72.9 ($^1J_{F,C}$ = 280 Hz, $^2J_{F,C}$ = 33 Hz). EI-MS (70 eV, 100 °C): m/z (intensity) 495 (100%) $[M]^+$,18 (66%) $[H_2O]^+$. Anal. Calcd for $C_{14}H_{15}F_3NOSIr$: C, 34.00; H, 3.06; N, 2.83; S, 6.48. Found: C, 34.92; H, 1.98; N, 3.01; S, 6.74.

CVD Experiments. Thin film deposition was performed in a horizontal cold-wall CVD reactor equipped with inductive field heating. The substrates (1 cm × 1 cm) were heated through a graphite susceptor. The molecular precursor was introduced to the reactor through a glass flange by applying a dynamic vacuum (10^{-3} mbar) and heating the precursor reservoir to the desired temperature. No carrier or reactive gases were used.[45] Hematite films were deposited by radio frequency plasma enhanced chemical vapor deposition (PE-CVD) onto FTO substrates using $Fe(CO)_5$ as the iron source and pure O_2 gas as the oxygen source, as reported elsewhere.[46−48] TiO_2 films were deposited via PECVD onto FTO substrates by using $Ti(O^iPr)_4$ as a precursor. The as-grown films were amorphous and were annealed for 2 h in air at 750 °C to obtain crystalline hematite films (α-Fe_2O_3) and 500 °C for TiO_2.

Materials Characterization. Room-temperature powder X-ray diffraction (XRD) was carried out on a STOE-STADI MP diffractometer operating in the reflection mode using Cu Kα (λ = 1.5406 Å) radiation. The microstructures of the samples were examined using field-emission scanning electron microscopy (FE-SEM, FEI Nova NanoSEM 430). PEC measurements were carried out in a three-electrode electrochemical cell with a 1.0 M NaOH electrolyte using a potentiostat (PAR Model Versa state IV, USA) and a 150 W xenon lamp (Oriel), which was equipped with an AM 1.5 filter to simulate the solar spectrum.

ASSOCIATED CONTENT

Supporting Information

The Supporting Information is available free of charge on the ACS Publications website at DOI: 10.1021/acs.organomet.7b00275.

DOI: 10.1021/acs.organomet.7b00275
Organometallics XXXX, XXX, XXX−XXX

NMR, EI mass spectra, an additional XRD pattern, SEM cross section images, and details of crystal and structure refinement (PDF)

Accession Codes

CCDC 1543504 contains the supplementary crystallographic data for this paper. These data can be obtained free of charge via www.ccdc.cam.ac.uk/data_request/cif, or by emailing data_request@ccdc.cam.ac.uk, or by contacting The Cambridge Crystallographic Data Centre, 12 Union Road, Cambridge CB2 1EZ, UK; fax: +44 1223 336033.

AUTHOR INFORMATION

Corresponding Author

*E-mail for S.M.: sanjay.mathur@uni-koeln.de.

ORCID

Lasse Jürgensen: 0000-0002-8385-9886

Sanjay Mathur: 0000-0003-2765-2693

Notes

The authors declare no competing financial interest.

ACKNOWLEDGMENTS

The authors gratefully acknowledge the University of Cologne and the Regional Research Cluster Sustainable Chemical Synthesis for financial support. We thank the German Science Foundation (DFG) for financial support in the frame of the priority programs "Manipulation of matter controlled by electric and magnetic fields: Towards novel synthesis and processing routes of inorganic materials" (SPP 1959), "Fuels Produced Regeneratively Through Light-Driven Water Splitting: Clarification of the Elemental Processes Involved and Prospects for Implementation in Technology Concepts" (SPP 1613) and the University of Cologne for providing infrastructure and financial assistance.

REFERENCES

(1) Mattinen, M.; Hämäläinen, J.; Vehkamäki, M.; Heikkilä, M. J.; Mizohata, K.; Jalkanen, P.; Räisänen, J.; Ritala, M.; Leskelä, M. *J. Phys. Chem. C* **2016**, *120*, 15235−15243.

(2) Jiang, X.; Huang, H.; Prinz, F. B.; Bent, S. F. *Chem. Mater.* **2008**, *20*, 3897−3905.

(3) Kaim, W.; Schwederski, B.; Klein, A. *Bioinorganic Chemistry: Inorganic Elements in the Chemistry of Life*; Wiley: Chichester, U.K., 2013.

(4) Carmo, M.; Fritz, D. L.; Mergel, J.; Stolten, D. *Int. J. Hydrogen Energy* **2013**, *38*, 4901−4934.

(5) An, J.; Kim, Y.-B.; Prinz, F. B. *Phys. Chem. Chem. Phys.* **2013**, *15*, 7520−7525.

(6) Hämäläinen, J.; Ritala, M.; Leskelä, M. *Chem. Mater.* **2014**, *26*, 786−801.

(7) Fabbri, E.; Habereder, A.; Waltar, K.; Kotz, R.; Schmidt, T. J. *Catal. Sci. Technol.* **2014**, *4*, 3800−3821.

(8) McCrory, C. C. L.; Jung, S.; Ferrer, I. M.; Chatman, S. M.; Peters, J. C.; Jaramillo, T. F. *J. Am. Chem. Soc.* **2015**, *137*, 4347−4357.

(9) Nong, H. N.; Gan, L.; Willinger, E.; Teschner, D.; Strasser, P. *Chem. Sci.* **2014**, *5*, 2955−2963.

(10) Felix, C.; Maiyalagan, T.; Pasupathi, S.; Bladergroen, B.; Linkov, V. *Micro Nanosyst.* **2012**, *4*, 186−191.

(11) Minguzzi, A.; Locatelli, C.; Lugaresi, O.; Achilli, E.; Cappelletti, G.; Scavini, M.; Coduri, M.; Masala, P.; Sacchi, B.; Vertova, A.; Ghigna, P.; Rondinini, S. *ACS Catal.* **2015**, *5*, 5104−5115.

(12) Oakton, E.; Lebedev, D.; Fedorov, A.; Krumeich, F.; Tillier, J.; Sereda, O.; Schmidt, T. J.; Coperet, C. *New J. Chem.* **2016**, *40*, 1834−1838.

(13) Sen, F. G.; Kinaci, A.; Narayanan, B.; Gray, S. K.; Davis, M. J.; Sankaranarayanan, S. K. R. S.; Chan, M. K. Y. *J. Mater. Chem. A* **2015**, *3*, 18970−18982.

(14) Cherevko, S.; Geiger, S.; Kaisan, O.; Mingers, A.; Mayrhofer, K. J. J. *J. Electroanal. Chem.* **2016**, *774*, 102−110.

(15) Abbott, D. F.; Lebedev, D.; Waltar, K.; Povia, M.; Nachtegaal, M.; Fabbri, E.; Coperet, C.; Schmidt, T. J. *Chem. Mater.* **2016**, *28*, 6591−6604.

(16) Serp, P.; Kalck, P. *Chem. Rev.* **2002**, *102*, 3085−3128.

(17) Vargas Garcia, J. R.; Goto, T. *Mater. Trans.* **2003**, *44*, 1717−1728.

(18) Mattinen, M.; Hämäläinen, J.; Gao, F.; Jalkanen, P.; Mizohata, K.; Räisänen, J.; Puurunen, R. L.; Ritala, M.; Leskelä, M. *Langmuir* **2016**, *32*, 10559−10569.

(19) Pyeon, M.; Wang, M.; Gönüllü, Y.; Kaouk, A.; Jaeckle, S.; Christiansen, S.; Hwang, T.; Moon, K.; Mathur, S. *MRS Commun.* **2016**, *6*, 442−448.

(20) Johnson, R. W.; Huldtqvist, A.; Bent, S. F. *Mater. Today* **2014**, *17*, 236−246.

(21) George, S. M. *Chem. Rev.* **2010**, *110*, 111−131.

(22) Igumenov, I. K. *J. Phys. IV* **1995**, *05*, C5-489−C5-496.

(23) Puddephatt, R. J. *Polyhedron* **1994**, *13*, 1233−1243.

(24) Hierso, J. C.; Feurer, R.; Kalck, P. *Coord. Chem. Rev.* **1998**, *178*−*180*, 1811−1834.

(25) Vasilyev, V. Y.; Morozova, N. B.; Basova, T. V.; Igumenov, I. K.; Hassan, A. *RSC Adv.* **2015**, *5*, 32034−32063.

(26) Schläfer, J.; Graf, D.; Fornalczyk, G.; Mettenbörger, A.; Mathur, S. *Inorg. Chem.* **2016**, *55*, 5422−5429.

(27) Appel, L.; Leduc, J.; Webster, C. L.; Ziller, J. W.; Evans, W. J.; Mathur, S. *Angew. Chem., Int. Ed.* **2015**, *54*, 2209−2213.

(28) Czympiel, L.; Pfrommer, J.; Tyrra, W.; Schäfer, M.; Mathur, S. *Inorg. Chem.* **2015**, *54*, 25−37.

(29) Appel, L.; Fiz, R.; Tyrra, W.; Pantenburg, I.; Mathur, S. *Cryst. Growth Des.* **2015**, *15*, 1141−1149.

(30) Leduc, J.; Ravithas, R.; Rathgeber, L.; Mathur, S. *New J. Chem.* **2015**, *39*, 7571−7574.

(31) Yamagata, T.; Nagata, M.; Mashima, K.; Tani, K. *Acta Crystallogr., Sect. E: Struct. Rep. Online* **2007**, *63*, m1498.

(32) Chen, Y.-L.; Liu, C.-S.; Chi, Y.; Carty, A. J.; Peng, S.-M.; Lee, G.-H. *Chem. Vap. Deposition* **2002**, *8*, 17−20.

(33) Sun, Y.-M.; Endle, J. P.; Smith, K.; Whaley, S.; Mahaffy, R.; Ekerdt, J. G.; White, J. M.; Hance, R. L. *Thin Solid Films* **1999**, *346*, 100−107.

(34) Le Formal, F.; Tétreault, N.; Cornuz, M.; Moehl, T.; Grätzel, M.; Sivule, K. *Chem. Sci.* **2011**, *2*, 737−743.

(35) Le Formal, F.; Grätzel, M.; Sivula, K. *Adv. Funct. Mater.* **2010**, *20*, 1099−1107.

(36) Tamirat, A. G.; Su, W.-N.; Dubale, A. A.; Chen, H.-M.; Hwang, B.-J. *J. Mater. Chem. A* **2015**, *3*, 5949−5961.

(37) Badia-Bou, L.; Mas-Marza, E.; Rodenas, P.; Barea, E. M.; Fabregat-Santiago, F.; Gimenez, S.; Peris, E.; Bisquert, J. *J. Phys. Chem. C* **2013**, *117*, 3826−3833.

(38) *Topspin*, Version 3.2, Bruker BioSpin GmbH, Rheinstetten, 2005.

(39) *X-RED32 1.31 and X-SHAPE 1.06*; Stoe & Cie, Darmstadt, Germany, 2005 and 1999.

(40) Farrugia, L. J. *J. Appl. Crystallogr.* **1999**, *32*, 837−838.

(41) Altomare, A.; Cascarano, G.; Giacovazzo, C.; Guagliardi, A. *J. Appl. Crystallogr.* **1994**, *27*, 435.

(42) Sheldrick, G. M. *Acta Crystallogr., Sect. A: Found. Crystallogr.* **2008**, *64*, 112−122.

(43) Spek, A. L. *J. Appl. Crystallogr.* **2003**, *36*, 7−13.

(44) Kawase, M.; Teshima, M.; Saito, S.; Tani, S. *Heterocycles* **1998**, *48*, 2103−2109.

(45) Veith, M.; Lecerf, N.; Mathur, S.; Shen, H.; Hüfner, S. *Chem. Mater.* **1999**, *11*, 3103−3112.

(46) Choi, T.; Hoffmann, M. *J. Phys. Chem.* **1994**, *98*, 13669.

(47) Singh, A.; Mettenbörger, A.; Golus, P.; Mathur, S. *Int. J. Hydrogen Energy* **2012**, *37*, 13983−13988.

DOI: 10.1021/acs.organomet.7b00275
Organometallics XXXX, XXX, XXX−XXX

(48) Kaouk, A.; Ruoko, T.-P.; Gönüllü, Y.; Kaunisto, K.; Mettenbörger, A.; Gurevich, E.; Lemmetyinen, H.; Ostendorf, A.; Mathur, S. *RSC Adv.* **2015**, *5*, 101401−101407.

DOI: 10.1021/acs.organomet.7b00275
Organometallics XXXX, XXX, XXX−XXX